EFFECT OF BAKING TEMPERATURE ON THE ALUMINUM SUBSTRATE FORMABILITY AND CORRELATION BETWEEN SUBSTRUCTURE AND TEXTURE EVOLUTION

Sofia M. Papadopoulou[1,2]*, Evangelos Gavalas[1], Spyros Papaefthymiou[2]

[1]Hellenic Research Centre for Metals (ELKEME), 61st km Athens-Lamia National Road, Oinofyta 32011, Greece

[2]National Technical University of Athens (NTUA), 9 Heroon Polytechniou Str., Zografou 15780, Greece

Abstract

In the present study, the effect of baking (painting) temperature on 3104 cold-rolled sheets for body stock application in terms of substructure and formability was examined. The thermal treatment performed during banking process provided optimum results towards the coating response and therefore its effect on the Al sheet deep drawability is examined. Mechanical testing in three directions, hardness measurements and microstructural analyses with optical microscopy and EBSD were applied and evaluated. In the current examination different painting soaking times were selected (10-20 s)on a 3104 aluminum alloy sheet sample of 55% thickness reduction percentage and it was found that the optimum mechanical properties are succeeded after heat treatment for 20 s at 170ºC, sample 4. In the resulting metallurgical condition the substructure was characterized by a high percentage of high angle grain boundaries (88%),while thee crystallographic deformation texture prevails an planar and vertical anisotropyexhibit acceptable results for the subsequent submission to a deep indentation process.

Keywords: *baking, AA3104, substructure, EBSD, anisotropy, formability*

1. INTRODUCTION

The Al alloys are characterized by many desired properties for everyday and special applications [1]-[5]. More specifically, alloy 3003 is used in cookware and chemical equipment due to its high anti-corrosion behavior, and alloy 3004 and its modification to alloy 3104 dominate the production of beverage and food containers. In addition, alloy 3105 is utilized for applications in architecture (building roofs and railway sidings) as well as in the automotive industry, and plant heat exchangers. Therefore, 3xxx series is one of the most used series of aluminum alloys which exceeds the values of 1.6 million tons per year [5], [6]. These products are mainly coated before forming in order to maintain and even enhance their naturally given advantages [2], [5], [7]-[9]. But except for the macroscopically observed properties (mechanical properties) [10], [11] and the grain structure, different aspect of the material play a crucial role in the material response and at the same time they have not been studied thoroughly [12], [13]. Therefore the ostensibly harmless baking thermal process may have a severe impact on the substructure and therefore on the later material response. The susceptible to theses processes regions are called sub-grains (Sub-grains/Cell blocks) [14]-[19], they are relatively equiaxed and characterized by misorientation angles with their neighboring sub-grains of the order of 1-5° (Low Angle Grain Boundaries, LAGB), while they are separated from each other from boundaries formed due to the accumulation of disturbances during deformation (Incidental Dislocation Boundaries, IDBs) [4], [12], [14]. The percentage of theses features influences the material response towards the mechanical behavior as well as the recrystallization force and therefore it is important to understand their evolution during this important and high added value process [15]-[19]. At the same time, the coating since it is polymer, it is subjected to other thermodynamic rules [17]. As it has been proven in study , the most beneficial for the coating behavior during forming are 170ºC and it is important to understand the effect of this temperature to the Al substrate as well.

2. MATERIALS AND METHODS

The AA 3104 alloy sheet samples (Table 1) that were examined were produced through direct chill (DC) casting and originated from a 600 mm thickness plate. Additionally, the sheet samples were subjected to hot and cold rolling as well as to thermal treatments.

Table 1. Chemical composition of the examined samples according to [24].

Elements (%)									
Al	**Mn**	**Mg**	**Fe**	**Si**	**Cu**	**Ti**	**Ga**	**V**	**Zn**
95.0-98.4	0.80-1.4	0.80-1.3	≤0.80	≤0.60	0.05-0.25	≤0.10	≤0.05	≤0.05	≤0.25

2.1. Selection of thermal treatment

In the present study the effect of different painting soaking times and temperatures affect the mechanical properties and microstructure of aluminum alloy 3104 sheet with a thickness of 0.20 mm. The study aims to find the optimal combination (of what????) as it simulates a factory-scale paint line. Considering information from other researchers as well as data from an actual factory paint line, 10, 15 and 20 s soaking time at 170oCwere selected for lab annealing [14], [17], [18] (Table 2). **Table 2.** Conditions selected for thermal treatments according to [14], [17], [18].

Sample ID	**T (°C)**	**t (s)**
1	**As received**	
2	170	10
3		15
4		20

2.2. Tensile Testing

The materials were subjected to uniaxial tensile strength, as per the requirements of the ISO 6892-1 testing standard. In particular, the Rp (yield strength—YS), Rm (ultimate tensile strength—UTS) and Ag (elongation) parameters were measured. The tensile strength specimens were cut, in orientations of 0°, 45° and 90° relevant to the RD.

The first way to quantify the anisotropy of AA3104 sheets - and each sheet - is to calculate the width to thickness ratio of the plastic deformation during the tensile test [34], [35]. This ratio is called the Lankford coefficient (r) and is a one-measure of the plastic anisotropy of rolled sheets and characterizes the susceptibility to forming of the rolled product [34]. The Lankford coefficient is calculated during the tensile test, either by using elongation meters or by digital image correlation (DIC) [35], based on the following equation [34]:

$$r = \frac{\epsilon_w}{\epsilon_t} = \left\{ \frac{\ln \frac{w}{w_0}}{\ln \frac{t}{t_0}} \right\} \quad (1.1)$$

, where ε_w is the true width deformation, ε_t is the true thickness deformation, w_0 is the initial width of the tensile specimen, t_0 is the initial thickness of the tensile specimen, w is the final width of the tensile

specimen and t is the final thickness of the tensile specimen. High values of the coefficient r indicate high resistance to thinning of the thickness direction [34].

However, the calculation of Lankford parameters for each of the directions (r_0, r_{45}, r_{90}) does not lead to a clear conclusion regarding the behavior of the plate during forming. For this reason, the parameter rm or is used, which is called "vertical anisotropy" ($\bar{r}$, normal anisotropy) and is a function of all three Lankford parameters as calculated from the relation [34]:

$$r_m = \bar{r} = \frac{(r_0 + r_{90} + 2r_{45})}{4} \quad (1.2)$$

The vertical anisotropy parameter describes the ability of the plate to shape in the direction of its thickness, relative to its surface, and is a parameter that is directly related to the limiting drawing ratio (LDR) parameter. For parameter values greater than one unit, the plate resists thinning, which is destructive to treatments such as deep drawing, while the larger the unit's parameter, the better the material's behavior during deep drawing (higher drawability). For values $\bar{r}$ smaller than the unit, the risk of failure of the sheet during its deep drawing increases [22]. Another parameter used to evaluate the anisotropy of sheets, such as AA3104, is that of planar anisotropy (Δr), which is calculated as a function of the Lankford parameters from the relation [23]:

$$\Delta r = \frac{(r_0 + r_{90} - 2r_{45})}{2} \quad (1.3)$$

The planar anisotropy parameter is an indicator of the ability of the rolled material not to show differential plastic deformation during the deep drawing on the perimeter of the produced cup, i.e. not to present the undesired phenomenon of "earing".

2.3. Optical Microscopy

Samples were sectioned parallel to the rolling direction and were cold mounted to avoid any non-desirable annealing effects. Metallographic preparation was conducted through successive grinding and polishing steps, whereas the grain structure was revealed through the use of Barker's electrolytic etching according to references [3,18]. Examination of the grain structure was performed with polarized light and by use of a Nikon Epiphot 300 inverted metallographic microscope (Nikon, Minato City, Tokyo, Japan). Optical metallographic examination was conducted at (probably 200x????) magnification.

2.4. Metallographic Examination—Texture

Microscopic analysis was performed using a JEOL IT-800 HL Scanning Electron Microscope (SEM, JEOL Ltd., Akishima, Tokyo, Japan) under 20 kV accelerating voltage, coupled with an EDAX Apollo XF, equivalent to octane super EDS, silicon drift detector (SDD, EDAX, Mahwah, NJ, USA) in conjunction with TEAM (EDAX, Mahwah, NJ, USA) and SMILE VIEW™ Map software (JEOL Ltd., Akishima, Tokyo, Japancity, and Digital Surf, Besançon, France). EBSD analysis was carried out using an EDAX Hikari XP EBSD, high-speed camera (EDAX camera, EDEN Instruments SAS, Valence Cedex, France). Calculation of the various texture components, resulting from the applied manufacturing process, was performed according to [19]:

-Rolling components: Copper {112}<111>, S2{213}<-1-42>, S3 (or S) {123}<634>, Taylor{4411}<11118>, Brass {011}<211>

-Recrystallization components: Cube {001}<100>, P{011}<111>, Q{013}<2-31>, R{124}<211>, Goss{011}<100>

EBSD scans were collected through a hexagonal grid. For the EBSD analysis, samples were examined in the as polished condition with a tilt of 70° relative to the electron beam and the step size was set at 0.1 μm to 1 μm depending on the material condition and the magnification used (100×–2000×) (examined areas 30 × 30 μm^2–150 × 150 μm^2). Points with low confidence index were excluded from

the texture measurements. Scanning data were analyzed by means of a post-processing software package (OIM) for the various texture components to be identified and calculated. The selected misorientation angles categories were 2°–5° (subgrain angle boundaries), 5°–15° (low-angle grain boundaries, LAGBs) and 15°–62.8° (high-angle grain boundaries, HAGBs). Grain orientation spread (GOS) maps were also constructed for a more complete microstructure characterization. Misorientation angles lower than 0.5° corresponding to dense dislocation density, are not considered reliable for evaluation purposes due to the angular resolution of the EBSD [20]. Finally, post-processing was conducted to clean up the data (grain dilation).

3. RESULTS

As observed in Fig 1, the microstructure is characterized by elongated grains towards the rolling direction. Regarding the different soaking times, no significant changes are observed in the morphology of the grains and this happens due to the short duration of time that characterizes each treatment.

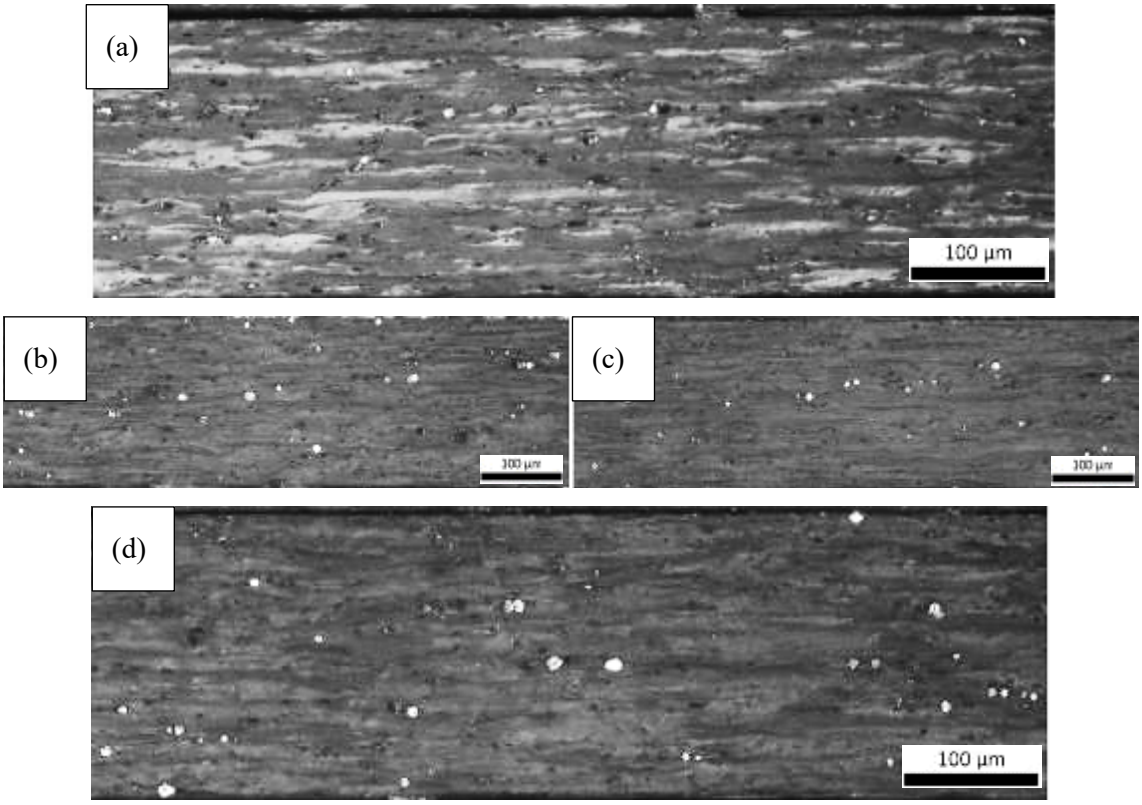


Figure 1. (a)-(d) Optical micrographs of the examined samples after Barkers electrolytic etching.

From the EBSD scans inverse pole figure (IPF) maps and misorientation angle grain boundaries maps were retrieved (Fig. 2). From the IPF maps it can be concluded that there are no significant differences regarding the preferred orientations (see relevant IPF plots). From the IPF plots it is evident that the grains were parallel to the direction <112> at the initial state and after the thermal treatment a fiber of direction is evolving. As for the misorientation maps, qualitatively HAGBs are increasing for up to 15 s thermal treatment and LAGBs are continuously decreased as the soaking time is increased as shown in Table 2 and Fig. 3 as well. The r values are given in Table 2. Samples 1 and 2 exhibited negative Δr values (-0.40 and -1.40 respectively) while sample 3 and 4 positive (0,55 and 0,30 respectively). As for r normal, the optimum results are obtained by sample 2 (2.0), sample 3 and 4 exhibited similar results (0.65 and 0.78 respectively) and the lower value was observed at sample 1 (0.46).

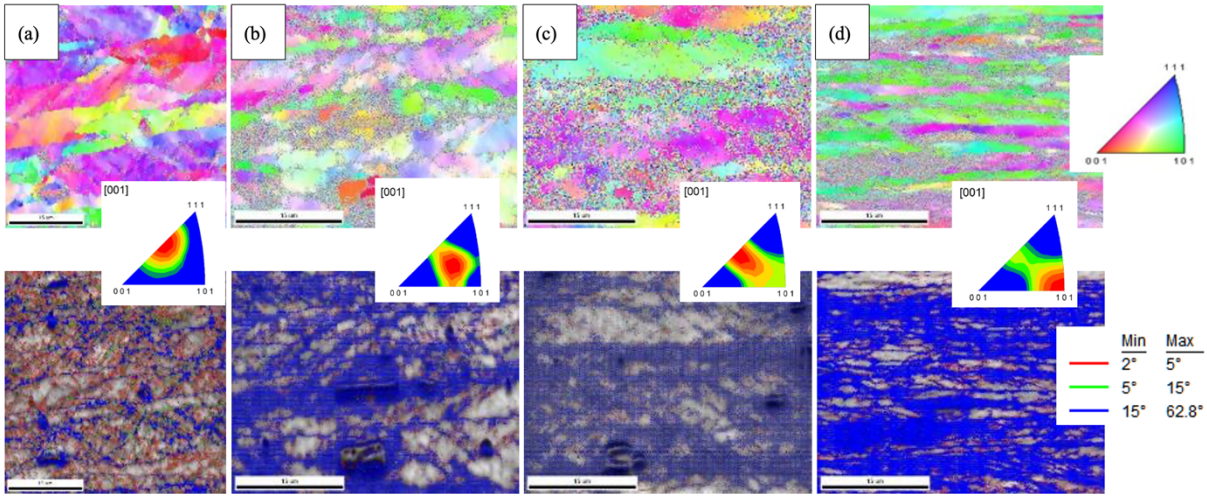


Figure 2. IPF maps, plots and misorientatation angle grain maps of samples (a) 1, (b) 2, (c) 3 and (d) 4.

Table 2. Results of misorientation angle grain boundaries percentages and r-values.

Sample ID	Misorientation angle boundaries (°)		*1Δr	*2$\bar{r}$
Sample 1	2°-5°	44.8	-0.40	0.46
	5°-15°	11.4		
	15° -62.8°	43.8		
Sample 2	2°-5°	11.9	-1.40	2.00
	5°-15°	3.3		
	15° -62.8°	84.8		
Sample 3	2°-5°	8.6	0.55	0.65
	5°-15°	2.7		
	15° -62.8°	88.7		
Sample 4	2°-5°	3.1	0.30	0.78
	5°-15°	2.8		
	15° -62.8°	88.1		

***1**: Planar anisotropy parameter/ is an indicator of the ability of a material to demonstrate a non-earing behavior (lower is better).

*2: Indicator of the ability of a material to be deep drawn (higher is better).

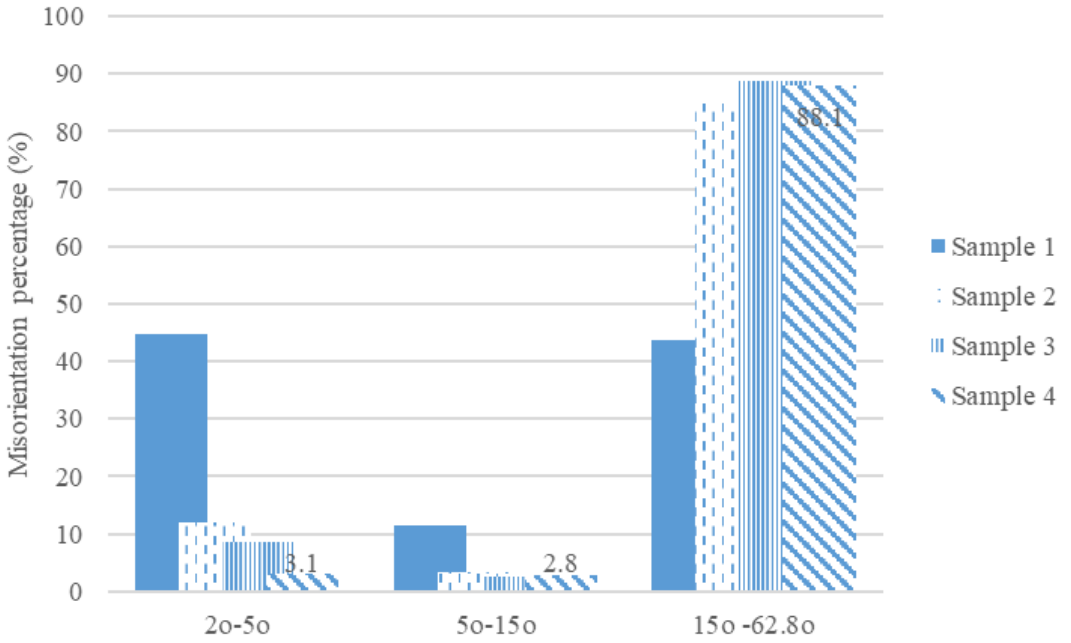


Figure 3. Histogram of misorientation angle percentages.

4. DISCUSSION

As plastic deformation progresses to higher levels the sub-grain blocks become very flat and are now separated from the plate-like dislocation zones (Lamellar Dislocation Boundaries, LBs), which have replaced the former boundaries. [1], [6],[4] The existence of geometrically necessary boundaries (GNBs) enables the rotation of the crystal lattice (Ω) to enable plastic deformation of the microstructure, which can originate from different slip systems acting between adjacent subgrain "blocks"[1]. Consequently, for moderate to large true deformations, a part of the geometrically necessary boundaries are characterized by misorientation angles greater than 10-15°, and now belong to the category of high angle boundaries, such as those characterizing grain boundaries (High Angle Grain Boundaries, HAGBs) [1], [4]. Simultaneously with the evolution of the microstructure during plastic deformation, where the aforementioned boundaries are formed due to the accumulation of perturbations in the microstructure, the preferred crystallographic texture characteristic of the applied deformation also evolves [34]. During the evolution of the crystallographic texture, large rotations of the crystal lattice of its grains of microstructure take place [34]. During these lattice rotations, different parts of a grain can be rotated to different final crystallographic orientations with high-angle boundaries (HAGBs) separating them [4].

The results presented in the study are indicative of the abovementioned statement since after cold-rolling the microstructure is characterized by an approximate 50% of sub grain boundaries and after the several thermal treatments this is gradually equalized with the other substructural features although the grain morphology remain stable.

Being areas of plastic instability, where the local plastic deformation is much larger compared to that practiced in the rest of the microstructure, they play an important role in the subsequent behavior of the metal material during its annealing as they are areas where the recrystallization phenomenon starts [1]. During recovery, the mechanically stored, in the form of dislocations, energy of the deformed microstructure decreases due to the increase in mobility of the dislocations, which either cancel each other out, if they are heteropolar, (Dislocation Annihilation) or rearrange into formations of lower energy (Dislocation Rearrangement) [14]. Therefore, in order to completely separate it from recrystallization, recovery is defined as the thermomechanical phenomenon that takes place during the annealing of deformed materials, without the migration of boundaries characterized by high misorientation angles (>15o), i.e. grain boundaries (HAGBs) [4].As can be seen, the restoration phenomenon includes

complex microstructural changes. As it can be concluded, the deformed state of the AA3104 sheets sample examined presented a high percentage of high angle grain boundaries accompanied by an equal amount of subgrain boundaries, fact that led to low response towards formability. Important to be noticed, is the enrichment of the in-between directions of <112> and <101> obtaining a more equilibrated composition of texture components and thus better mechanical response. The optimum results were retrieved when the highest amount of high angle grain boundaries was observed. Actual industrial products with different soaking times could be examined and further support the present results.

5. CONCLUSIONS

By examining the different painting soaking times on a 3104 aluminum alloy sheet sample of 55% thickness reduction percentage, it was found that the optimum mechanical properties of the product are during painting for 10 s at 170^{o}C where the substructure was characterized by a high percentage of high angle grain boundaries. In the given conditions the crystallographic deformation texture prevails as in the other examined samples, but there is a significant difference in the values of planar and vertical anisotropy which compared to the other examined conditions lead to much better results for the subsequent submission to a deep indentation process.

ACKNOWLEDGMENTS

The authors would like to express their gratitude to ELKEME S.A. and ELVAL S.A. management for all the kind support.

REFERENCES

1. G. Totten and D. MacKenzie, Handbook of aluminum. New York: Marcel Dekker, 2003, pp. 1, 38, 351, 352.
2. I. Polmear, Light alloys. Oxford: Elsevier/Butterworth-Heinemann, 2006, pp. 115.
3. J. Davis, ASM Specialty Handbook, Aluminum and aluminum alloys. Materials Park, OH: ASM International, 1993, pp. 18, 21, 44, 231.
4. R. D. Doherty et al., “Current issues in recrystallization: A review,” Mater. Today, vol. 1, no. 2, pp. 14–15, 1998, doi: 10.1016/s1369-7021(98)80046-1.
5. S. Papadopoulou, A. Kontopoulou, E. Gavalas, and S. Papaefthymiou. 2020. "The Effects of Reduction and Thermal Treatment on the Recrystallization and Crystallographic Texture Evolution of 5182 Aluminum Alloy" Metals 10, no. 10: 1380. https://doi.org/10.3390/met10101380.
6. J. Kaufman, Introduction to aluminum alloys and tempers. Materials Park, OH: ASM International, 2000, pp. 11, 27, 90.
7. "How and why alloying elements are added to aluminum", Alcotec.com, 2021. [Online]. Available: http://www.alcotec.com/us/en/education/knowledge/qa/How-and-why-alloying-elements-are-added-to-aluminum.cfm.
8. W. Callister and D. Rethwisch, Materials Science And Engineering An Introduction, 8th ed. 2010, pp. 213, 215, 212, 417.
9. G. Dieter and D. Bacon, Mechanical metallurgy. London: McGraw-Hill, 1988, pp. 203, 232, 589.
10. C. Gandhi, "Effect Of Homogenization On The Microstructural Development In A D.C. Cast AA3104 Aluminum Alloy Used For Canbody Stock", Master Of Applied Science, Indian Institute of Technology, 1994.

11. D. Magidi and L. Tessa, "The Study Of Intermetallic Particles In Aluminium Alloy AA3104 Can-Body Stock During Homogenisation", Masters of Mathematical Science, University of Cape Town, 2017.
12. S. Papadopoulou, E. Gavalas, and S. Papaefthymiou. 2021. "Methodology for the Identification of Nucleation Sites in Aluminum Alloy by Use of Misorientatation Mapping" Materials Proceedings 3, no. 1: 11. https://doi.org/10.3390/IEC2M-09251.
13. S. Papadopoulou, V. Loukadakis, Z. Zacharopoulos, and S. Papaefthymiou. 2021. "Influence of Uniaxial Deformation on Texture Evolution and Anisotropy of 3104 Al Sheet with Different Initial Microstructure" Metals 11, no. 11: 1729. https://doi.org/10.3390/met11111729.
14. M. Groover, Fundamentals of Modern Manufacturing Materials, Processes and Systems, 4th ed. New York: Wiley, 2015, pp. 388, 384, 390, 396, 399.
15. R. Singh, Introduction to basic manufacturing processes and workshop technology. New Delhi: New Age Internation Publishers, 2006, pp. 282, 283.
16. A. Shahani, S. Setayeshi, S. Nodamaie, M. Asadi and S. Rezaie, "Prediction of influence parameters on the hot rolling process using finite element method and neural network", Journal of Materials Processing Technology, vol. 209, no. 4, pp. 1920-1935, 2009.
17. N. Hattori, M. Tanigawa and M. Okido, "Effect of baked temperature on the coating film formability of pre-coated aluminum sheets under drawing", Journal of Japan Institute of Light Metals, Vol. 56, No. 8, 2006, pp. 448–453.
18. "Safety Data Sheet Epoxy Topcoat, OSHA Hazard Communication Standard 29 CFR 1910.1200, Sterling Lacquer Mfg. Co.", P11.secure.hostingprod.com, 2016. [Online]. Available: https://p11.secure.hostingprod.com/@site.skygeek.com/ssl/MSDS/sterling-lacquer-22-11202qtkt-sterling-lacquer-22-11202-aluminum-epoxy-coating-kit-mil-c-22750.pdf.
19. J. Black and R. Kohser, De Garmo's Materials and Processes in Manifacturing, 10th ed. New York, N.Y.: Wiley, 2007, pp. 382.
20. S. Semiatin and D. Furrer, "Simulation of Microstructure and Texture Evolution in Aluminum Sheet", 2009.
21. A. Lise Dons, "The Alstruc homogenization model for industrial aluminum alloys", Journal of Light Metals, vol. 1, no. 2, pp. 133-149, 2001. Available: 10.1016/s1471-5317(01)00007-4.
22. J. Martin, Concise encyclopedia of materials processing. Amsterdam: Elsevier, 2009.
23. F. Humphreys and M. Hatherly, Recrystallization and Related Annealing Phenomena. Elsevier, 2004.
24. https://www.matweb.com/search/datasheet_print.aspx?matguid=aaaabe41a20a4ed2b48270f7f2ef1b2d
25. V. Randle and O. Engler, "Introduction to Texture Analysis, Macrotexture, Microtexture and Orientation Mapping", 2010. Available: 10.1201/9781482287479.
26. A. Rollett, "Microstructure and Anisotropy", 2014.
27. M. Rout, S. Pal and S. Singh, "Cross Rolling: A Metal Forming Process, Modern Manufacturing Engineering", Materials Forming, Machining and Tribology, pp. 41-64, 2015. Available: 10.1007/978-3-319-20152-8_2.
28. O. Engler, L. Löchte and K. Karhausen, "Modelling of Recrystallisation Kinetics and Texture during the Thermo-Mechanical Processing of Aluminium Sheets", Materials Science Forum, vol. 495-497, pp. 555-566, 2005. Available: 10.4028/www.scientific.net/msf.495-497.555.
29. A. Schwartz, M. Kumar and B. Adams, Electron backscatter diffraction in materials science. New York: Springer, 2009.

30. J. Hirsch and T. Al-Samman, "Superior light metals by texture engineering: Optimized aluminum and magnesium alloys for automotive applications", Acta Materialia, vol. 61, no. 3, pp. 818-843, 2013. Available: 10.1016/j.actamat.2012.10.044.
31. J. Hirsch and O. Engler, "Texture, local orientation and microstructure in industrial Al alloys, Microstructural and Crystalographic Aspects of Recrystallization", 1995.
32. J. Davis, Tensile testing. Materials Park, Ohio: ASM International, 2004.
33. S. Suwas and R. Ray, Crystallographic Texture of Materials. London: Springer, 2014.
34. S. Wright and M. Nowell, "EBSD Image Quality Mapping", Microscopy and Microanalysis, vol. 12, no. 01, pp. 72-84, 2006. Available: 10.1017/s1431927606060090.
35. "Standard Test Method for Tensile Strain – Hardening Exponents (n – Values) of Metallic Sheet Materials, ASTM, United States ", Astm.org, 2021. [Online]. Available: https://www.astm.org/Standards/E646.htm.
36. "Standard Test Method for Plastic Strain Ratio r for Sheet Metal, ASTM, Designation E 517-00, United States", Astm.org, 2021. [Online]. Available: https://www.astm.org/Standards/E517.htm.
37. R. Huang, Z. Yin, Q. Huang and M. Liao, "The Influence of Composition on the Material Structure and Performance of 3104 Aluminum-Alloy Canbody Material", Advanced Materials Research, vol. 535-537, pp. 987-991, 2012. Available: 10.4028/www.scientific.net/amr.535-537.987.
38. O. Engler and K. Knarbakk, "Temper rolling to control texture and earing in aluminium alloy AA 5050A", 2020. [Online]. Available: https://www.researchgate.net/publication/344847991_Temper_rolling_to_control_texture_and_earing_in_aluminium_alloy_AA_5050A.
39. P. Oldring and U. Nehring, "Packaging Materials, Metal Packaging For Foodstuffs, International Life Sciences Institute", Pac.gr, 2007. [Online]. Available: https://www.pac.gr/bcm/uploads/7-metal-packaging-for-foodstuffs.pdf.